

Path Planning for image based control with omnidirectional cameras

Hicham Hadj-Abdelkader, Youcef Mezouar and Philippe Martinet

Abstract—Image-based servoing is a local control solution, it requires thus the definition of intermediate subgoals in the sensor space when the robot initial position is far away from the desired one. This issue is crucial when using omnidirectional cameras since very large motions can be achieved. This paper addresses the problem of generating smooth trajectories in the image space of the entire class of central cameras (including conventional perspective cameras). The model of the observed target is assumed to be unknown. First geometrical relationships between imaged points and lines in two views are exploited to estimate a generic homography matrix. A closed-form homography path between given start and end-points is then derived and used to generate the trajectories of image features. Results obtained with real data are finally presented.

I. INTRODUCTION

Image-based servoing is now a well known local control framework. In this approach, the reference image of the object corresponding to a desired position of the robot is acquired first (during an off-line step) and some image features are extracted. Features extracted from the initial image are matched with those obtained from the desired one. These features are then tracked during the robot (and/or the object) motion, using for example a correlation based method. An error is obtained by comparing the image features in the current image and in the reference one. The robot motion is then controlled in order to minimize the error (using for example a gradient descent approach). Since the error is directly measured in the image, image-based servo has some degrees of robustness with respect to modelling errors and noise perturbations. However, sometimes, and especially when the initial and desired configurations are distant, the trajectories induced by image-based servo are neither physically valid nor optimal due to the nonlinearity and singularities in the relation from the image space to the workspace. Dealing with this deficiency, path planning in the image-space is a promising approach. Indeed, if the initial error is too large, a reference trajectory can be designed from a sequence of images. The initial error can thus be sampled so that, at each iteration of the control loop, the error to regulate remains small. In [11], relay images that interpolate initial and reference image features using an affine approximation of the relationship between initial and desired images, coupled to a potential switching control scheme, are proposed to enlarge the stable region. In [12], a trajectory generator using a stereo system is proposed and applied to obstacle avoidance. An alignment task for an 4 DOF robot using intermediate views of the object synthesized by image

morphing is presented in [21]. A path planning for a straight-line robot translation observed by a weakly calibrated stereo system is performed in [20]. In [15], a potential field-based path planning generator that determines the trajectories in the image of a set of points lying on an unknown target has been proposed. To increase the stability region, Cowan and Koditschek in [5] describe a globally stabilizing method using navigation function for eye-to-hand setup. However, none of these works were dealing with optimality issues. In [23], a numerical framework for the design of optimal trajectories in the image space is described and applied to the simple case of a one dimensional camera in a two dimensional workspace. In [16], the problem of finding the trajectories in the image space of 3D points imaged with a conventional perspective camera corresponding to optimal 3D camera trajectories is addressed. In this paper, we extend this framework to the entire class of central catadioptric cameras. Indeed when using such a sensor this issue is crucial since the motions that can be realized by the robot are very large.

There is significant motivations for using central catadioptric cameras. Indeed conventional cameras suffer from restricted field of view. Many applications in vision-based robotics, such as mobile robot localization and navigation, can benefit from panoramic field of view provided by omnidirectional cameras. In the literature, there have been several methods proposed for increasing the field of view of cameras systems. One effective way is to combine mirrors with conventional imaging system. The obtained sensors are referred as catadioptric imaging systems. The resulting imaging systems have been termed central catadioptric when a single projection center describes the world-image mapping. From a theoretical and practical view point, a single center of projection is a desirable property for an imaging system [2]. Clearly, visual servoing applications can also benefit from such sensors since they naturally overcome the visibility constraint. Vision-based control of robotic arms, single mobile robot or formation of mobile robots appear thus in the literature with omnidirectional cameras (refer for example to [4], [19],[17]). Image-based visual servoing with central catadioptric cameras using points has been studied in [4], [9]. The use of straight lines has also been investigated in [17], [10].

The above mentioned control schemes are local control solutions as when using a conventional perspective camera. Furthermore, omnidirectional cameras can be used to realize much more larger displacement since they can provide a larger view of the environment. In this case path planning should not be considered as optional and should be inte-

LASMEA
24, avenue des Landais, 63177 Aubiere Cedex, France
{hadj,mezouar,martinet}@univ-bpclermont.fr

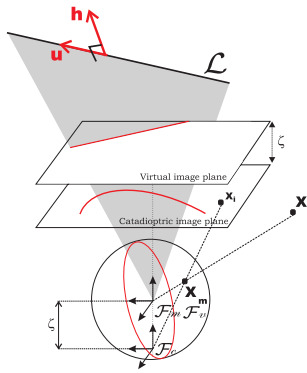


Fig. 1. Central catadioptric image formation

grated. This paper addresses this issue. A solution to plan the trajectories of features directly in the image space of central catadioptric cameras is proposed. The structure from motion problem using imaged 3D points and lines (conics) is firstly studied. Geometrical relationship between two views are exploited to linearly estimate a generic homography matrix. A smooth closed-form homography path between two given points is then obtained and the trajectories of the image features corresponding to minimal length camera trajectories are derived.

II. CENTRAL CATADIOPTRIC IMAGING MODEL

The central catadioptric projection can be modeled by a central projection onto a virtual unitary sphere, followed by a perspective projection onto an image plane. This virtual unitary sphere is centered in the principal effective view point and the image plane is attached to the perspective camera. In this model, called unified model and proposed by Geyer and Daniilidis in [7], conventional perspective camera appears as a particular case.

A. Projection of point

Let \mathcal{F}_c and \mathcal{F}_m be the frames attached to the conventional camera and to the mirror respectively. In the sequel, we suppose that \mathcal{F}_c and \mathcal{F}_m are related by a simple translation along the Z -axis (\mathcal{F}_c and \mathcal{F}_m have the same orientation as depicted in Figure 1). The origins C and M of \mathcal{F}_c and \mathcal{F}_m will be termed optical center and principal projection center respectively. The optical center C has coordinates $[0 \ 0 \ -\xi]^T$ with respect to \mathcal{F}_m and the image plane $Z = f(\psi - 2\xi)$ is orthogonal to the Z -axis where f is the focal length of the conventional camera and ξ and ψ describe the type of sensor and the shape of the mirror, and are function of mirror shape parameters (refer to [3]).

Consider the virtual unitary sphere centered in M as shown in Fig.1 and let \mathcal{X} be a 3D point with coordinates $\mathbf{X} = [X \ Y \ Z]^T$ with respect to \mathcal{F}_m . The world point \mathcal{X} is projected in the image plane into the point of homogeneous coordinates $\mathbf{x}_i = [x_i \ y_i \ 1]^T$. The image formation process can be split in three steps as:

- **First step:** The 3D world point \mathcal{X} is first projected on the unit sphere surface into a point of

coordinates in \mathcal{F}_m : $\mathbf{X}_m = \frac{1}{\sigma} [X \ Y \ Z]^T$, where $\sigma = \|\mathbf{X}\| = \sqrt{X^2 + Y^2 + Z^2}$. The projective ray \mathbf{X}_m passes through the principal projection center M and the world point \mathcal{X} .

- **Second step:** The point \mathbf{X}_m lying on the unitary sphere is then perspective projected on the normalized image plane $Z = 1 - \xi$. This projection is a point of homogeneous coordinates $\underline{\mathbf{x}} = [\mathbf{x}^T \ 1]^T = \mathbf{f}(\mathbf{X})$ (where $\mathbf{x} = [x \ y]^T$):

$$\underline{\mathbf{x}} = \mathbf{f}(\mathbf{X}) = \left[\begin{array}{ccc} X & Y & \\ Z + \xi\sigma & Z + \xi\sigma & 1 \end{array} \right]^T \quad (1)$$

- **Third step:** Finally the point of homogeneous coordinates $\underline{\mathbf{x}}_i$ in the image plane is obtained after a plane-to-plane collineation \mathbf{K} of the 2D projective point \mathbf{x} : $\mathbf{x}_i = \mathbf{K}\underline{\mathbf{x}}$. The matrix \mathbf{K} can be written as $\mathbf{K} = \mathbf{K}_c\mathbf{M}$ where the upper triangular matrix \mathbf{K}_c contains the conventional camera intrinsic parameters, and the diagonal matrix \mathbf{M} contains the mirror intrinsic parameters:

$$\mathbf{M} = \begin{bmatrix} \psi - \xi & 0 & 0 \\ 0 & \psi - \xi & 0 \\ 0 & 0 & 1 \end{bmatrix}, \quad \mathbf{K}_c = \begin{bmatrix} f_u & \alpha_{uv} & u_0 \\ 0 & f_v & v_0 \\ 0 & 0 & 1 \end{bmatrix}$$

Note that, setting $\xi = 0$, the general projection model becomes the well known perspective projection model.

In the sequel, we assume that $Z \neq 0$. Let us denote $\eta = s\sigma/|Z| = s\sqrt{1 + X^2/Z^2 + Y^2/Z^2}$, where s is the sign of Z . The coordinates of the image point can be rewritten as:

$$x = \frac{X/Z}{1 + \xi\eta}; \quad y = \frac{Y/Z}{1 + \xi\eta}$$

By combining the two previous equations, it is easy to show that η is the solution of the following second order equation:

$$\eta^2 - (x + y)^2(1 + \xi\eta)^2 - 1 = 0$$

with the following potential solutions:

$$\eta_{1,2} = \frac{\pm\gamma - \xi(x^2 + y^2)}{\xi^2(x^2 + y^2) - 1} \quad (2)$$

where $\gamma = \sqrt{1 + (1 - \xi^2)(x^2 + y^2)}$. Note that, the sign of η is equal to the sign of Z and then it can be shown (refer to Appendix) that the exact solution is:

$$\eta = \frac{-\gamma - \xi(x^2 + y^2)}{\xi^2(x^2 + y^2) - 1} \quad (3)$$

Equation (3) shows that η can be computed as a function of image coordinates \mathbf{x} and sensor parameter ξ . Noticing that:

$$\mathbf{X}_m = (\eta^{-1} + \xi)\bar{\mathbf{x}} \quad (4)$$

where $\bar{\mathbf{x}} = [\mathbf{x}^T \frac{1}{1 + \xi\eta}]^T$, we deduce that \mathbf{X}_m can also be computed as a function of image coordinates \mathbf{x} and sensor parameter ξ .

B. Projection of lines

Let \mathcal{L} be a 3D straight line in space lying on the interpretation plane which contains the principal projection center M (see Figure 1). The binormalized Euclidean Plücker coordinates [1] of the 3D line are defined as $[\bar{\mathbf{u}}^T \ \bar{\mathbf{h}}^T \ h]^T$. The unit vectors $\bar{\mathbf{h}} = (h_x, h_y, h_z)^T$ and $\bar{\mathbf{u}} = (u_x, u_y, u_z)^T$ are respectively the orthogonal vector to the interpretation plane and the orientation of the 3D line \mathcal{L} and are expressed in the mirror frame \mathcal{F}_m . h is the distance from \mathcal{L} to the origin of the definition frame. The unit vectors $\bar{\mathbf{h}}$ and $\bar{\mathbf{u}}$ are orthogonal, thus verify $\bar{\mathbf{h}}^T \bar{\mathbf{u}} = 0$. If the 3D line is imaged with a perspective camera then the unit vector $\bar{\mathbf{h}}$ contains the coefficient of the 2D line \mathbf{l} in the image plane, i.e the homogeneous coordinates \mathbf{x} of the perspective projection of any world point lying on \mathcal{L} verifies:

$$(\mathbf{K}^{-T} \bar{\mathbf{h}})^T \mathbf{x} = \mathbf{l}^T \mathbf{x} = 0 \quad (5)$$

with $\mathbf{l} = \mathbf{K}^{-T} \bar{\mathbf{h}}$. If the line is imaged with a central catadioptric camera then the 3D points on the 3D line \mathcal{L} are mapped into points \mathbf{x} in the catadioptric image lying on a conic curve:

$$\mathbf{x}^T \mathbf{K}^{-T} \boldsymbol{\Omega} \mathbf{K}^{-1} \mathbf{x} = \mathbf{x}^T \boldsymbol{\Omega}_i \mathbf{x} = 0 \quad (6)$$

where $\boldsymbol{\Omega}_i = \mathbf{K}^{-T} \boldsymbol{\Omega} \mathbf{K}^{-1}$ and:

$$\boldsymbol{\Omega} \propto \begin{bmatrix} h_x^2 - \xi^2(1 - h_y^2) & h_x h_y (1 - \xi^2) & h_x h_z \\ h_x h_y (1 - \xi^2) & h_y^2 - \xi^2(1 - h_x^2) & h_y h_z \\ h_x h_z & h_y h_z & h_z^2 \end{bmatrix}$$

C. Polar lines

The quadratic equation (6) is defined by five coefficients. Nevertheless, the catadioptric image of a 3D line has only two degrees of freedom. In the sequel, we show how we can get a minimal representation using polar lines.

Let Φ , A be respectively a 2D conic curve, a point in the definition plane of Φ . The polar line \mathbf{l} of A with respect to Φ is defined by $\mathbf{l} \propto \Phi A$. Now, consider the principal point $\mathbf{O}_i = [u_0 \ v_0 \ 1]^T = \mathbf{K}[0 \ 0 \ 1]^T$ and the polar line \mathbf{l}_i of \mathbf{O}_i with respect to $\boldsymbol{\Omega}_i$: $\mathbf{l}_i \propto \boldsymbol{\Omega}_i \mathbf{O}_i$, then:

$$\begin{aligned} \mathbf{l}_i &\propto \mathbf{K}^{-T} \boldsymbol{\Omega} \mathbf{K}^{-1} \mathbf{O}_i = \mathbf{K}^{-T} \boldsymbol{\Omega} \mathbf{K}^{-1} \mathbf{K}[0 \ 0 \ 1]^T \\ &\propto \mathbf{K}^{-T} \bar{\mathbf{h}} \end{aligned} \quad (7)$$

Moreover, equation (7) yields:

$$\bar{\mathbf{h}} = \frac{\mathbf{K}^T \mathbf{l}_i}{\|\mathbf{K}^T \mathbf{l}_i\|} \quad (8)$$

It is thus clear that the polar line \mathbf{l}_i contains the coordinates of the projection of the 3D line \mathcal{L} in an image plane of an equivalent (virtual) perspective camera defined by the frame $\mathcal{F}_v = \mathcal{F}_m$ (see figure 1) with internal parameters chosen equal to the internal parameters of the catadioptric camera (i.e $\mathbf{K}_v = \mathbf{K}_c \mathbf{M}$). This result is fundamental since it allows us to represent the physical projection of a 3D line in a catadioptric camera by a simple (polar) line in a virtual perspective camera rather than a conic. Knowing only the optical center \mathbf{O}_i , it is thus possible to use the linear pin-hole model for the projection of a 3D line instead of the non linear central catadioptric projection model.

III. SCALED EUCLIDEAN RECONSTRUCTION USING HOMOGRAPHY MATRIX OF CATADIOPTRIC VISION

Several methods were proposed to obtain Euclidean reconstruction from two views [6]. They are generally based on the estimation of the fundamental matrix [14] in pixel space or on the estimation of the essential matrix [13] in normalized space. However, for control purposes, the methods based on the essential matrix are not well suited since degenerate configurations can occur (such as pure rotational motion). Homography matrix and Essential matrix based approaches do not share the same degenerate configurations, for example pure rotational motion is not a degenerate configuration when using homography-based method. The epipolar geometry of central catadioptric system has been more recently investigated [8], [22]. The central catadioptric fundamental and essential matrices share similar degenerate configurations that those observed with conventional perspective cameras, it is why we will focus on homographic relationship. In the sequel, the collineation matrix \mathbf{K} and the mirror parameter ξ are supposed known. To estimate these parameters the algorithm proposed in [3] can be used. In the next section, we show how we can compute homographic relationships between two central catadioptric views of co-planar points and co-planar lines.

Let \mathbf{R} and \mathbf{t} be the rotation matrix and the translation vector between two positions \mathcal{F}_m and \mathcal{F}_m^* of the central catadioptric camera (see Figures 2 and 3). Consider a 3D reference plane (π) given in \mathcal{F}_m^* by the vector $\pi^{*\top} = [\mathbf{n}^* \ -d^*]$, where \mathbf{n}^* is its unitary normal in \mathcal{F}_m^* and d^* is the distance from (π) to the origin of \mathcal{F}_m^* .

A. Homography matrix from points

Let \mathcal{X} be a 3D point with coordinates $\mathbf{X} = [X \ Y \ Z]^T$ with respect to \mathcal{F}_m and with coordinates $\mathbf{X}^* = [X^* \ Y^* \ Z^*]^T$ with respect to \mathcal{F}_m^* . Its projection in the unit sphere for the two camera positions are:

$$\mathbf{X}_m = (\eta^{-1} + \xi) \bar{\mathbf{x}} = \frac{1}{\rho} [X \ Y \ Z]^T$$

$$\mathbf{X}_m^* = (\eta^{*-1} + \xi) \bar{\mathbf{x}}^* = \frac{1}{\rho} [X^* \ Y^* \ Z^*]^T$$

Using the homogenous coordinates $\underline{\mathbf{X}} = [X \ Y \ Z \ H]^T$ and $\underline{\mathbf{X}}^* = [X^* \ Y^* \ Z^* \ H^*]^T$, we can write:

$$\rho(\eta^{-1} + \xi) \bar{\mathbf{x}} = [\mathbf{I}_3 \ 0] \underline{\mathbf{X}} = [\mathbf{R} \ \mathbf{t}] \underline{\mathbf{X}}^* \quad (9)$$

The distance $d(\mathcal{X}, \pi)$ from the world point \mathcal{X} to the plane (π) is given by the scalar product $\pi^{*\top} \cdot \underline{\mathbf{X}}^*$ and:

$$d(\mathbf{X}^*, \pi^*) = \rho^*(\eta^{*-1} + \xi) \mathbf{n}^{*\top} \bar{\mathbf{x}}^* - d^* H^*$$

As a consequence, the unknown homogenous component H^* is given by:

$$H^* = \frac{\rho^*(\eta^{*-1} + \xi)}{d^*} \mathbf{n}^{*\top} \bar{\mathbf{x}}^* - \frac{d(\mathbf{X}^*, \pi^*)}{d^*} \quad (10)$$

The homogeneous coordinates of \mathcal{X} with respect to \mathcal{F}_m^* can be rewritten as:

$$\underline{\mathbf{X}}^* = \rho^*(\eta^{*-1} + \xi) [\mathbf{I}_3 \ 0]^T \bar{\mathbf{x}}^* + [\mathbf{0}_{1 \times 3} \ H^*]^T \quad (11)$$

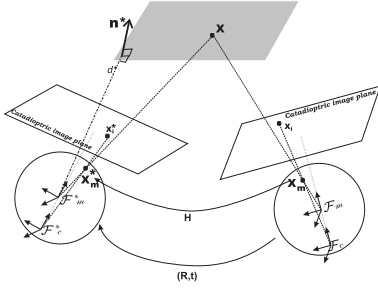


Fig. 2. Geometry of two views of points

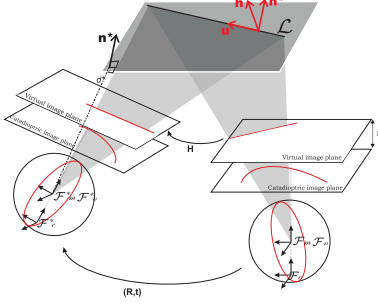


Fig. 3. Geometry of two views of lines

By combining the Equations (10) and (11), we obtain:

$$\underline{\mathbf{X}}^* = \rho^*(\eta^{*-1} + \xi)\mathbf{A}^*\bar{\mathbf{x}}^* + \mathbf{b}^* \quad (12)$$

where

$$\mathbf{A}_\pi^* = \left[\mathbf{I}_3 \quad \frac{\mathbf{n}^*}{d^*} \right]^\top \quad \text{and} \quad \mathbf{b}_\pi^* = \left[\mathbf{0}_{1 \times 3} \quad -\frac{d(\mathcal{X}, \pi)}{d^*} \right]$$

According to (12), the expression (9) can be rewritten as:

$$\rho(\eta^{-1} + \xi)\bar{\mathbf{x}} = \rho^*(\eta^{*-1} + \xi)\mathbf{H}\bar{\mathbf{x}}^* + \alpha \mathbf{t} \quad (13)$$

with $\mathbf{H} = \mathbf{R} + \frac{\mathbf{t}}{d^*}\mathbf{n}^{*T}$ and $\alpha = -\frac{d(\mathcal{X}, \pi)}{d^*}$.

\mathbf{H} is the Euclidean homography matrix written as a function of the camera displacement and of the plane coordinates with respect to \mathcal{F}_m^* . It has the same form as in the conventional perspective case (it is decomposed into a rotation matrix and a rank 1 matrix). If the world point \mathcal{X} belongs to the reference plane (π) (i.e. $\alpha = 0$) then Equation (13) becomes:

$$\bar{\mathbf{x}} \propto \mathbf{H}\bar{\mathbf{x}}^* \quad (14)$$

B. Homography matrix from lines

Let \mathcal{L} be a 3D straight line with binormalized Euclidean Plücker coordinates $[\bar{\mathbf{u}}^\top \bar{\mathbf{h}}^\top h]^\top$ with respect to \mathcal{F}_m and with coordinates $[\bar{\mathbf{u}}^{*\top} \bar{\mathbf{h}}^{*\top} h^*]^\top$ with respect to \mathcal{F}_m^* . Consider that the 3D line \mathcal{L} lies in a 3D reference plane (π) as defined below.

Let \mathcal{X}_1 and \mathcal{X}_2 be two points in the 3D space lying on the line \mathcal{L} . The central catadioptric projection of the 3D line \mathcal{L} is fully defined by the normal vector to the interpretation plane $\bar{\mathbf{h}}$. The vector $\bar{\mathbf{h}}$ can be defined by two points in the 3D line as $\bar{\mathbf{h}} = \frac{\mathbf{X}_1 \times \mathbf{X}_2}{\|\mathbf{X}_1 \times \mathbf{X}_2\|}$. Noticing

that $[\mathbf{H}\mathbf{X}_1^*]_\times = \det(\mathbf{H})\mathbf{H}^{-\top}[\mathbf{X}_1^*]_\times\mathbf{H}^{-1}$ ($[\mathbf{H}\mathbf{X}_1^*]_\times$ being the skew-symmetric matrix associated to the vector $\mathbf{H}\mathbf{X}_1^*$) and according to (4) and (14), $\bar{\mathbf{h}}$ can be written as:

$$\bar{\mathbf{h}} \propto \frac{\det(\mathbf{H})}{\|\mathbf{X}_1^* \times \mathbf{X}_2^*\|} \mathbf{H}^{-\top}(\mathbf{X}_1^* \times \mathbf{X}_2^*)$$

Since $\bar{\mathbf{h}}^* = \frac{\mathbf{X}_1^* \times \mathbf{X}_2^*}{\|\mathbf{X}_1^* \times \mathbf{X}_2^*\|}$ is the normal vector to the interpretation plane expressed in the frame \mathcal{F}_m^* , the relationship between two views of the 3D line can be written by:

$$\bar{\mathbf{h}} \propto \mathbf{H}^{-\top} \bar{\mathbf{h}}^* \quad (15)$$

The expression of the homography matrix in the pixel space can be derived hence using the polar lines. As depicted below, each conic, corresponding to the projection of a 3D line in the omnidirectional image, can be explored through its polar line. Let \mathbf{l}_i and \mathbf{l}_i^* be the polar lines of the image center \mathbf{O}_i with respect to the conics Ω_i and Ω_i^* respectively in the two positions \mathcal{F}_m and \mathcal{F}_m^* of the catadioptric camera. From equation (7), the relationship given in equation (15) can be rewritten as:

$$\mathbf{l}_i \propto \mathbf{G}^{-\top} \mathbf{l}_i^* \quad (16)$$

where $\mathbf{G} = \mathbf{K}\mathbf{H}\mathbf{K}^{-1} = \mathbf{K}(\mathbf{R} + \frac{\mathbf{t}}{d^*}\mathbf{n}^{*T})\mathbf{K}^{-1}$.

Note that the homography matrix related to (π) can be linearly estimated using points or lines. When points are used, the equation (14) can be tuned into a linear homogeneous equation: $\bar{\mathbf{x}} \times \mathbf{H}\bar{\mathbf{x}}^* = \mathbf{0}$ (where \times denotes the cross-product) and thus \mathbf{H} can be estimated up to a scale factor, using four couples of coordinates $(\mathbf{x}_k; \mathbf{x}_k^*)$, $k = 1 \dots 4$, corresponding to the projection in the normalized image space of world points \mathcal{X}_k belonging to (π). When lines are used, equation (16) can be rewritten as: $\mathbf{l}_i \times \mathbf{G}^{-\top} \mathbf{l}_i^* = \mathbf{0}$, \mathbf{G} can thus be estimated using at least four couples of coordinates $(\mathbf{l}_{ik}, \mathbf{l}_{ik}^*)$, $k = 1 \dots 4$. The homography matrix is then computed as $\mathbf{H} = \mathbf{K}^{-1}\mathbf{G}\mathbf{K}$.

In both cases (points or lines visual), the camera motion parameters \mathbf{R} , $\mathbf{t}_{d^*}^* = \frac{\mathbf{t}}{d^*}$ and the structure of the observed scene (for example the vector \mathbf{n}^*) can be determined from the estimated Euclidean homography matrix (refer to [6], [24]).

IV. PATH PLANNING IN THE CATADIOPTIC IMAGE SPACE

In the sequel, the current position of the camera with respect to its desired position is given by the rotation matrix $\mathbf{R}(t)$ and the scaled translational vector $\mathbf{t}_{d^*}(t) = \frac{\mathbf{t}(t)}{d^*}$. In this case, the homography matrix is $\mathbf{H}(t) \propto \mathbf{R}(t) + \mathbf{t}_{d^*}(t)\mathbf{n}^{*T}$. We assume that the initial image (\mathcal{I}_0 at time $t = 0$) and the final image (\mathcal{I}_1 at time $t = 1$) corresponding to the initial and desired robot positions are available. From the extracted image features the homography matrix \mathbf{H}_0 , at time $t = 0$, can be computed. The rotation matrix \mathbf{R}_0 , the scaled translational vector \mathbf{t}_{0d^*} and the normal vector \mathbf{n}^{*T} can then be extracted from \mathbf{H}_0 . Note also that, when the desired configuration is reached (at time $t = 1$), the homography matrix is proportional to the identity matrix: $\mathbf{H}_1 \propto \mathbf{I}$, and this configuration corresponds to $\mathbf{R}_1 = \mathbf{I}$ and $\mathbf{t}_{d^*}(1) = \mathbf{0}$.

The paths of \mathbf{R} in $S(3)$ and of \mathbf{t} in \mathcal{R}^3 corresponding to a minimal length camera trajectory are given by [18]:

$$\mathbf{t}(t) = (1 - q(t))\mathbf{t}_0 \quad \text{and} \quad \mathbf{R}(t) = \mathbf{R}_0 e^{[\boldsymbol{\theta}_0]q(t)} \quad (17)$$

where $[\boldsymbol{\theta}_0] = \log(\mathbf{R}_0^\top) = \frac{\theta_0}{2 \sin \theta_0} (\mathbf{R}_0^\top - \mathbf{R}_0)$ (θ_0 is the rotation angle computed from \mathbf{R}_0^\top), $q(t)$ is a polynomial such that $q(0) = 0$ and $q(1) = 1$. The polynomial $q(t)$ can be chosen in order that equation (17) corresponds to the solutions of the minimum energy problem (*i.e.*, if \mathbf{U} denotes a vector containing the six components of the camera velocity equation (17) corresponds to the solution which minimizes $J = \int_0^1 \mathbf{U}^\top \mathbf{U} dt$ if $q(t) = t$) or of the minimum acceleration problem (*i.e.*, equation (17) corresponds to the solution which minimizes $J = \int_0^1 \dot{\mathbf{U}}^\top \dot{\mathbf{U}} dt$ if $q(t) = -2t^3 + 3t^2$) [18]. According to equations (17), the path of the homography matrix is given by:

$$\mathbf{H}(t) = \mathbf{R}_0 e^{[\boldsymbol{\theta}_0]q(t)} + (1 - q(t))\mathbf{t}_{0d^*} \mathbf{n}^{*\top} \quad (18)$$

Knowing start points, the trajectories of imaged points between \mathcal{I}_0 and \mathcal{I}_1 can now be obtained by combining equations (14) and (18). The trajectories of polar lines can be derived from equations (16) and (18). Since there is a one-to-one mapping between polar lines and the matrix representation of imaged lines (conics), one can deduce the trajectories of the conic curve in the image space from the trajectories of the polar lines (refer to equation (7) and (8)).

V. RESULTS

In this section, we present two experiments of the proposed path planning scheme with catadioptric camera. In the first experiment points have been used as visual features and in the second one, the trajectories of imaged lines (conics) have been planned. In these experiments, a calibrated paracatadioptric camera (parabolic mirror combined with an orthographic lens) is used.

A. Points visual features

In this first experiment, points features are extracted from the catadioptric image of a checkerboard. The images corresponding to the initial and final positions of the catadioptric camera are given in figures 4 and 5 respectively. The catadioptric camera displacement between initial and final images is very large. The trajectories in the catadioptric image space given in figure 5 correspond to the solution of the minimum energy problem (*i.e.* $q(t) = t$). Figure ?? shows the corresponding camera trajectories. Note that only the temporal behavior is different when choosing a different polynomial $q(t)$.

B. Lines visual features

In this experiment, conics features are extracted from the catadioptric image (refer to figures 6(a) and 6(b)). Polar lines associated to the principal point with respect to the extracted conics, are used to calculate the collineation matrix between the initial and final positions of the catadioptric camera. The images corresponding to the initial and final positions of the catadioptric camera are given in figures 6(a) and 6(b)

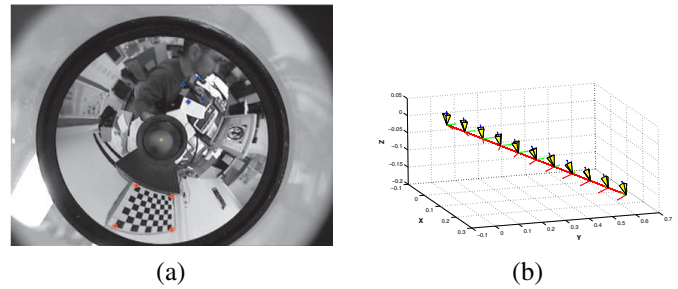


Fig. 4. (a) Initial image, (b) camera trajectory (minimum energy)

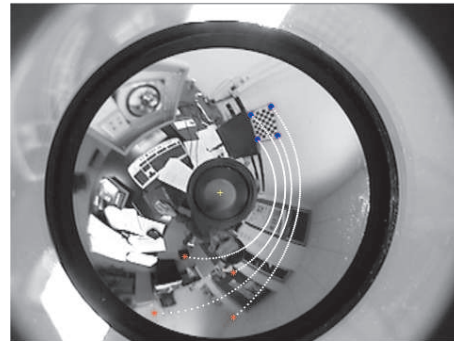


Fig. 5. Final/trajectories images.

respectively. The catadioptric camera displacement between initial and final images is very large. The trajectories of the conics in the catadioptric image space are showed in figure 6(b) (the polynomial $q(t)$ has been set to t). Figure ?? shows the corresponding camera trajectory.

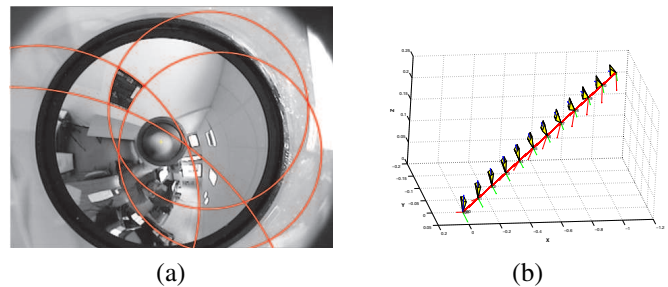


Fig. 6. (a) Initial image, (b) camera trajectory (minimum energy)

VI. CONCLUSIONS AND FUTURE WORKS

Since Image-based servoing is a local control solution, it requires the definition of intermediate subgoals in the sensor space. In this paper, we have addressed the problem of finding the trajectories of visual features imaged through central cameras corresponding to a minimal camera trajectory. The model of the observed target is not required in the proposed approach. First geometrical relationships between imaged points and lines in two views have been investigated and exploited to derive a closed-form homography path between given start and end-points. It was then possible to generate the trajectories of image features. We have finally validated the method with real data. A natural perspective

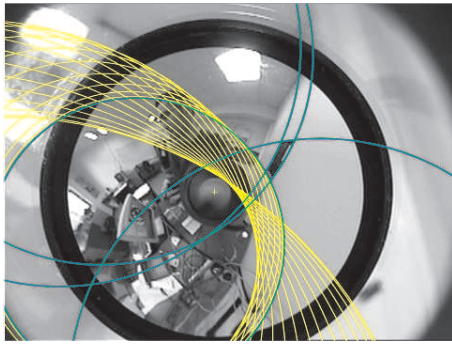


Fig. 7. Final/trajectories images.

for this work is the incorporation of obstacle avoidance in the path planning process as well as the incorporation of non-holonomic constraints.

APPENDIX

η (given by equation (3)) has the sign s of Z if the sign of its denominator is $-s$ since its numerator is always negative.

Let \mathcal{C}^+ , \mathcal{C}^0 and \mathcal{C}^- be three sub-spaces of the world defined by $Z > 0$, $Z = 0$ and $Z < 0$ respectively.

Any 3D points in the world space is projected in the normalized catadioptric image plane into the point of homogeneous coordinates $[x \ y \ 1]^T$. Consider $r = \sqrt{x^2 + y^2}$ (refer to figure 8). A 3D point of the sub-space \mathcal{C}^+ (respectively \mathcal{C}^0 and \mathcal{C}^-) is projected into an image point of coordinates $[x_+ \ y_+ \ 1]^T$ (respectively $[x_0 \ y_0 \ 1]^T$ and $[x_- \ y_- \ 1]^T$). It is clear that $r_+ < r_0 < r_-$ with $r_+ = \sqrt{x_+^2 + y_+^2}$ ($r_0 = \sqrt{x_0^2 + y_0^2}$ and $r_- = \sqrt{x_-^2 + y_-^2}$). As depicted in figure (8), $r_0 = \frac{1}{\xi}$ and it is easy to show that:

$$\begin{aligned} \text{if } Z > 0 &\Rightarrow r_+ < r_0 & \text{and} & \text{if } Z < 0 &\Rightarrow r_- > r_0 \\ &\Rightarrow \eta > 0 & & &\Rightarrow \eta < 0 \end{aligned}$$

Hence, η has the sign of Z .

REFERENCES

- [1] N. Andreff, B. Espiau, and R. Horaud. Visual servoing from lines. *International Journal of Robotics Research*, 21(8):679–700, August 2002.
- [2] S. Baker and S. K. Nayar. A theory of single-viewpoint catadioptric image formation. *International Journal of Computer Vision*, 35(2):1–22, November 1999.
- [3] J. Barreto and H. Araujo. Geometric properties of central catadioptric line images. In *7th European Conference on Computer Vision, ECCV'02*, pages 237–251, Copenhagen, Denmark, May 2002.
- [4] J. P. Barreto, F. Martin, and R. Horaud. Visual servoing/tracking using central catadioptric images. In *ISER2002 - 8th International Symposium on Experimental Robotics*, pages 863–869, Bombay, India, July 2002.
- [5] Noah J. Cowan, Joel D. Weingarten, and Daniel E. Koditschek. Visual servoing via navigation functions. *IEEE Transactions on Robotics and Automation*, 18(4):521–533, August 2002.
- [6] O. Faugeras and F. Lustman. Motion and structure from motion in a piecewise planar environment. *Int. Journal of Pattern Recognition and Artificial Intelligence*, 2(3):485–508, 1988.
- [7] C. Geyer and K. Daniilidis. A unifying theory for central panoramic systems and practical implications. In *European Conference on Computer Vision*, volume 29, pages 159–179, Dublin, Ireland, May 2000.
- [8] C. Geyer and K. Daniilidis. Mirrors in motion: Epipolar geometry and motion estimation. In *International Conference on Computer Vision, ICCV'03*, pages 766–773, Nice, France, 2003.
- [9] H. Hadj Abdelkader, Y. Mezouar, N. Andreff, and P. Martinet. 2 1/2 d visual servoing with central catadioptric cameras. In *IEEE/RSJ Int. Conf. on Intelligent Robots and Systems, IROS'05*, pages 2342–2347, Edmonton, Canada, August 2005.
- [10] H. Hadj Abdelkader, Y. Mezouar, N. Andreff, and P. Martinet. Omnidirectional visual servoing from polar lines. In *IEEE Int. Conf. on Robotics and Automation, ICRA'06*, Orlando, USA, May 2006.
- [11] K. Hashimoto and T. Noritugu. Potential switching control in visual servo. In *IEEE Int. Conf. on Robotics and Automation*, pages 2765–2770, San Francisco, USA, April 2000.
- [12] K. Hosoda, K. Sakamoto, and M. Asada. Trajectory generation for obstacle avoidance of uncalibrated stereo visual servoing without 3d reconstruction. *IEEE/RSJ Int. Conf. on Intelligent Robots and Systems*, 1(3):29–34, August 1995.
- [13] H.C. Longuet-Higgins. A computer algorithm for reconstructing a scene from two projections. *Nature*, 293:133–135, September 1981.
- [14] Quang-Tuan Luong and Olivier Faugeras. The fundamental matrix: theory, algorithms, and stability analysis. *Int. Journal of Computer Vision*, 17(1):43–76, 1996.
- [15] Y. Mezouar and F. Chaumette. Path planning for robust image-based control. *IEEE Transactions on Robotics and Automation*, 18(4):534–549, August 2002.
- [16] Y. Mezouar and F. Chaumette. Optimal camera trajectory with image-based control. *Int. Journal of Robotics Research*, 22(10):781–804, October 2003.
- [17] Y. Mezouar, H. Haj Abdelkader, P. Martinet, and F. Chaumette. Central catadioptric visual servoing from 3d straight lines. In *IEEE/RSJ Int. Conf. on Intelligent Robots and Systems, IROS'04*, volume 1, pages 343–349, Sendai, Japan, September 2004.
- [18] F. C Park and B. Ravani. Smooth invariant interpolation of rotations. *ACM Transactions on Graphics*, 16(3):277–295, July 1997.
- [19] A. Paulino and H. Araujo. Multiple robots in geometric formation: Control structure and sensing. In *International Symposium on Intelligent Robotic Systems*, pages 103–112, University of Reading, UK, July 2000.
- [20] A. Ruf and R. Horaud. Visual trajectories from uncalibrated stereo. *IEEE Int. Conf. on Intelligent Robots and Systems*, pages 83–91, September 1997.
- [21] R. Singh, R. M. Voyle, D. Littau, and N. P. Papanikolopoulos. Alignment of an eye-in-hand system to real objects using virtual images. *Workshop on Robust Vision for Vision-Based Control of Motion, IEEE Int. Conf. on Robotics and Automation*, May 1998.
- [22] Tomas Pajdla, Tomas Svoboda, and Vaclav Hlavac. Motion estimation using central panoramic cameras. In *IEEE Conference on Intelligent Vehicles*, Stuttgart, Germany, October 1998.
- [23] Hong Zhang and Jim Ostrowski. Optimal motion planning in the image plane for mobile robots. In *IEEE Int. Conf. on Robotics and Automation*, San Francisco, USA, April 2000.
- [24] Z. Zhang and A. R. Hanson. Scaled euclidean 3d reconstruction based on externally uncalibrated cameras. In *IEEE Symposium on Computer Vision*, Coral Gables, FL, 1995.

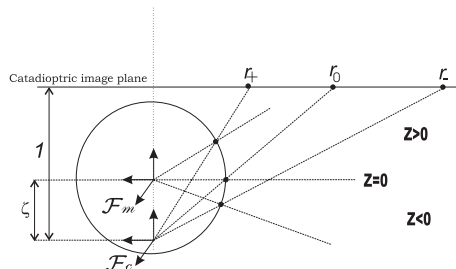


Fig. 8. view.